Journal of Catalysis **185,** 73–90 (1999)
Article ID jcat.1999.2481, available online at http://www.idealibrary.com on IDEAL®

Deuterium Pulse Transient Analysis for Determination of Heterogeneous Ethylene Hydroformylation Mechanistic Parameters

Scott A. Hedrick, Steven S. C. Chuang,[1] and Mark A. Brundage[2]

Department of Chemical Engineering, The University of Akron, Akron, Ohio 44325-3906

Received September 25, 1998; revised March 15, 1999; accepted March 15, 1999

Deuterium isotopic pulse tracing has been combined with *in situ* infrared spectroscopy to study heterogeneous ethylene hydroformylation and hydrogenation on a 4 wt% Mn–Rh/SiO_2 catalyst at 513 K and 0.1 MPa. Deuterium pulses into steady-state $CO/H_2/C_2H_4$ flow produced H_2, HD, D_2, $C_2H_{6-x}D_x$, and $C_2H_{6-x}D_xCO$ transient responses. The reaction parameters, including intermediate surface coverages and rate coefficients, were determined from the transient responses coupled with compartment models that describe adsorbed intermediates in the pathway for incorporation of D_2 into propionaldehyde. This pathway is shown below:

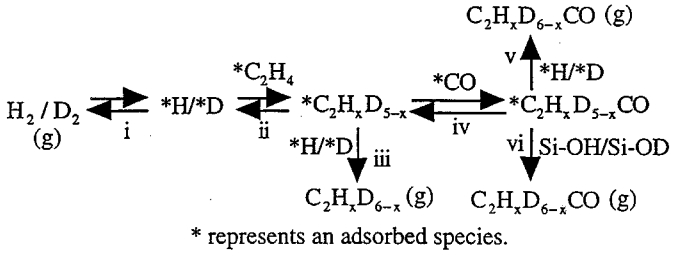

* represents an adsorbed species.

The pathway involves (i) deuterium adsorption, (ii) partial deuteration of adsorbed ethylene to form adsorbed ethyl, (iii) deuteration of adsorbed ethyl to form ethane, (iv) CO insertion into adsorbed ethyl to form adsorbed acyl, (v) deuteration of adsorbed acyl via metal-chemisorbed deuterium to form propionaldehyde, and (vi) deuteration of adsorbed acyl via spillover deuterium to form propionaldehyde. The steady-state rate of hydrogen desorption, which is essential for determination of the reaction parameters, was estimated by use of the HD transient response assuming that the rate of HD production equals the rate of D_2 production and equals the rate of H_2 production at the point where the surface coverages of H and D are approximately equal. Evaluation of rate coefficients indicates that hydrogenation of adsorbed ethyl is intrinsically faster than CO insertion into ethyl, leading to the high selectivity toward ethane over propionaldehyde as product. The propionaldehyde compartment models were able to account for two modes of acyl hydrogenation: (i) from *H on the metal surface and (ii) from spillover *H, or Si–OH. Hydrogenation via metal-adsorbed hydrogen is favored over hydrogenation via spillover hydrogen. Comparison of the rate coefficients for CO insertion and acyl hydrogenation indicates that both steps are kinetically significant, which is consistent with conclusions of previous studies that utilized the Langmuir–Hinshelwood–Hougen–Watson and pseudo-steady-state analysis approaches.

Key Words: **SSITKA; hydroformylation; hydrogenation; isotopic tracing; compartment modeling; *in situ* IR; spillover; transient studies; deuterium pulse tracing.**

INTRODUCTION

The goal of catalysis research is to use mechanistic information to guide the design and preparation of highly active and selective catalysts (1). One method that has been developed to gain insight into the nature of reactions on catalyst surfaces is *in situ* infrared (IR) spectroscopy coupled with steady-state isotopic transient kinetic analysis (SSITKA) (2). SSITKA involves the replacement of a reactant with its isotopically labeled counterpart, typically in the form of a step or pulse function. Producing an input function with isotope-labeled reactant permits the monitoring of isotopic transient responses while keeping the total concentration of labeled plus nonlabeled reactants, adsorbates, and products at steady-state conditions. The responses of the labeled reactants and products to the step or pulse input carry mechanistic information about the steady-state reaction. Isotopic transient techniques have been used in the past primarily to study CO hydrogenation (3–11) to obtain intermediate surface coverages and adsorbate activities for carbon-containing species such as carbides, $*CH_x$, *CO, $*C_2O$, $*C_2OH$, etc. (* denotes a chemisorbed species). The isotopic tracing technique, along with other similar isotope exchange experiments, has also been used to study ethylene hydrogenation to determine rate parameters for the Horiuti–Polanyi mechanism and the D_2–C_2H_4 exchange reaction (12, 13).

This study utilizes SSITKA coupled with *in situ* IR for the study of heterogeneous ethylene hydroformylation, which is the reaction of syngas with ethylene to form propionaldehyde as the desired product and ethane as the byproduct. Hydroformylation serves as a useful probe reaction for examination of hydrogenation and CO insertion activity

[1] To whom correspondence should be addressed. E-mail: schuang@uakron.edu. Fax: (330) 972-5856.

[2] Present address: General Motors, Rochester, NY.

0021-9517/99 $30.00

of transition metal catalysts (14). Our previous studies used ^{13}CO to trace the CO pathway and obtain mechanistic information, including elementary rate constants for carbon-containing intermediates and determination of the rate-limiting step on Rh/SiO_2 and $Mn–Rh/SiO_2$ catalysts (15–18). Deuterium transient studies have been conducted on Rh/SiO_2 to characterize temperature effects on propionaldehyde formation (19) and on $Mn–Rh/SiO_2$ to characterize (i) product readsorption effects, (ii) deuterium distribution in the products, and (iii) deuteration pathways to explain the two-hump d_i-propionaldehyde responses (18, 20).

Previous deuterium transient studies do not explicitly address steady-state hydrogen surface coverages under reaction conditions and very few contain quantitative determination of hydrogen adsorption–desorption rates. Obtaining these mechanistic parameters is not straightforward; it requires proper assumptions and the use of an appropriate model to fit the transient response data.

The objective of this study is to investigate the effect of reactant partial pressure on the mechanistic parameters, i.e., the rate of hydrogen adsorption–desorption, intermediate surface coverages, residence times, and reactivities of hydrogen and hydrogen-containing intermediates during the $H_2/CO/C_2H_4$ reaction on a 4 wt% $Mn–Rh/SiO_2$ catalyst. The mechanistic parameters will be determined by the transient responses of H_2, HD, D_2, and deuterium-containing products coupled with compartment models of hydroformylation.

EXPERIMENTAL

Catalyst Preparation and Characterization

A 4 wt% $Mn–Rh/SiO_2$ (Mn : Rh = 0.1) catalyst was prepared by a sequential incipient wetness method using an aqueous solution of $RhCl_3 \cdot 3H_2O$ (Alfa Products) and an aqueous solution of $Mn(NO_3)_2 \cdot 6H_2O$ onto a large pore SiO_2 support (Strem Chemicals, surface area of 350 m^2/g). Upon completion of the impregnation sequence, the catalyst powder was dried in air overnight at room temperature and then was reduced in flowing H_2 at 673 K for 16 h. Hydrogen uptake at room temperature was determined, via the flow chemisorption method, to be 114 $\mu mol/g_{cat}$, corresponding to a Rh particle size of 1.6 nm assuming an adsorption stoichiometry of $H_{ad} : Rh_{site} = 1$.

Reaction Studies

Specific details of the experimental apparatus and IR reactor cell used in this study have been reported elsewhere (2), but will be briefly described here. Approximately 50 mg of catalyst was used. One half of this total was pressed into a thin, self-supporting disk and used in the IR reactor where it was subject to the infrared beam. The remainder of the catalyst was placed at the reactor outlet for the purpose of increasing conversion. The IR cell acts as a differential reactor (conversion never exceeds 5%) and provides the initial rates for the forward reaction.

The reaction was carried out at 513 K and 0.1 MPa with a total flow rate of 120 cm^3/min. The reactant mixture consisted of H_2, CO, C_2H_4, and He. The H_2 stream consisted of 2 vol% Ar, which acted as an inert tracer to determine the flow pattern in the reactor system without interacting with the catalyst surface. The partial pressure of each reactant was varied four times while the other reactants' partial pressures remained constant for a total of twelve runs. Partial pressures were varied by altering the flow rate of each respective reactant as well as that of He in order to keep the total flow constant. Upon reaching steady-state flow at the desired conditions, an HP-5980A gas chromatograph (GC) equipped with a flame ionization detector (FID) and Porapak PS/Porapak QS columns in series was used to determine the steady-state concentrations of reactants and products. A six-port valve was then used to pulse 10 cm^3 of D_2 into the H_2 stream. After the pulse, IR spectra were recorded by a Nicolet 5SXC spectrometer with a DTGS detector (4 cm^{-1} resolution) in order to monitor transient responses of adsorbates on the catalyst surface. The transient responses of the gaseous effluent were simultaneously recorded by a Balzers QMG 112 mass spectrometer (MS) interfaced to a computer that allows measurement of eight m/e (i.e., amu) as a function of time. The m/e ratios monitored were 2 (H_2), 3 (HD), 4 (D_2), 30 (d_2-ethylene/d_0-ethane), 31 (d_3-ethylene/d_1-ethane), 32 (d_4-ethylene/d_2-ethane), 33 (d_3-ethane), 40 (Ar), 58 (d_0-propionaldehyde), 59 (d_1-propionaldehyde), 60 (d_2-propionaldehyde), and 61 (d_3-propionaldehyde). The d_i-prefix indicates the number of deuterium atoms in the molecule. Each experiment was performed twice at each condition to allow information to be gathered about all 12 species.

RESULTS

Steady-State Reaction Measurements

Figure 1 shows the steady-state turnover frequency (TOF) versus partial pressure for the major products: ethane and propionaldehyde. TOF is defined as the rate of product formation ($mol/g_{cat}/s$) divided by the number of surface Rh atoms per gram of catalyst measured by H_2 pulse chemisorption at room temperature. Only trace amounts of other hydrocarbons were produced. A best-fit of the rate versus partial pressure data yields the following empirical power–law relationships:

$$TOF_{C_2H_6} = 6.20 P_{H_2}^{1.20} P_{CO}^{-0.67} P_{C_2H_4}^{0.83} \quad [1]$$

and

$$TOF_{C_2H_5CHO} = 1.30 P_{H_2}^{0.85} P_{CO}^{0.14} P_{C_2H_4}^{0.84}. \quad [2]$$

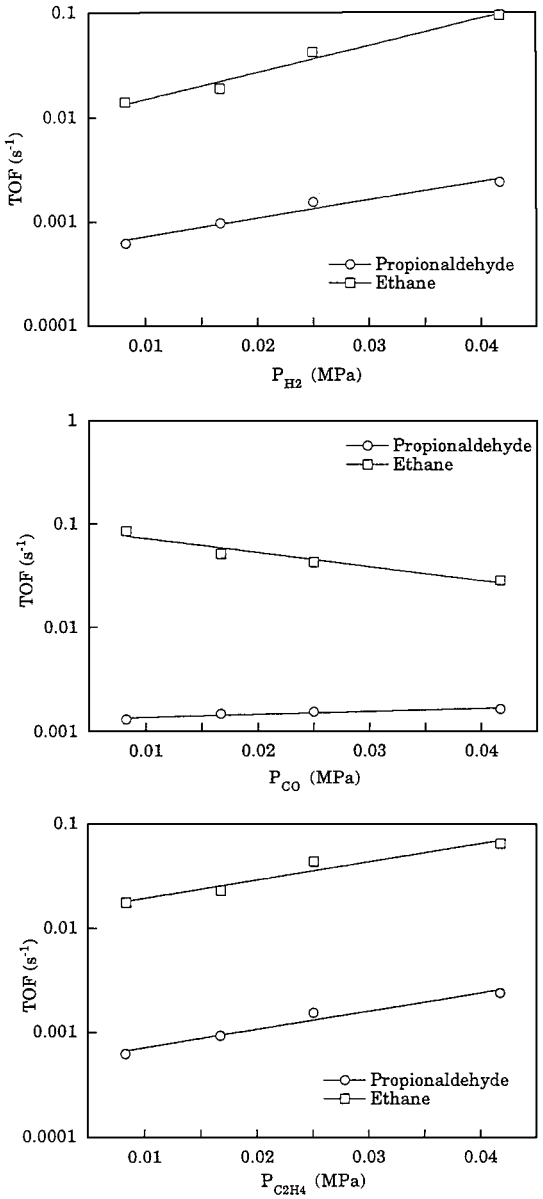

FIG. 1. TOF of ethane and propionaldehyde versus reactant partial pressure.

The reaction order shows the extent of the dependence of the product formation rate on the reactant partial pressure (MPa). The ethane formation rate shows positive order with respect to hydrogen and ethylene partial pressures and negative order with respect to CO partial pressure. Propionaldehyde formation rate shows positive order with respect to all reactants.

Comparison of ethane and propionaldehyde rates versus reactant partial pressure shows that the selectivity toward propionaldehyde increases with increasing CO partial pressure and decreases with increasing H_2 partial pressure. Increases in ethylene partial pressure had little impact on product selectivity.

Transient Response to a D_2 Pulse

Figure 2 shows the normalized reactant and product responses to a 10 cm^3 D_2 pulse into $H_2/CO/C_2H_4$/He flow at 30/30/30/30 cm^3/min. The responses were normalized using the equation (21)

$$E(t) = \frac{I(t)}{\int_0^\infty I(t)\,dt}, \qquad [3]$$

where $I(t)$ is the MS intensity for a specific gaseous species. $I(t)$ can be related to concentration of the species via a calibration factor. The normalization procedure described by Eq. [3] converts all the MS responses such that the area under each curve is one; this allows for fair comparison of the lead–lag relationships.

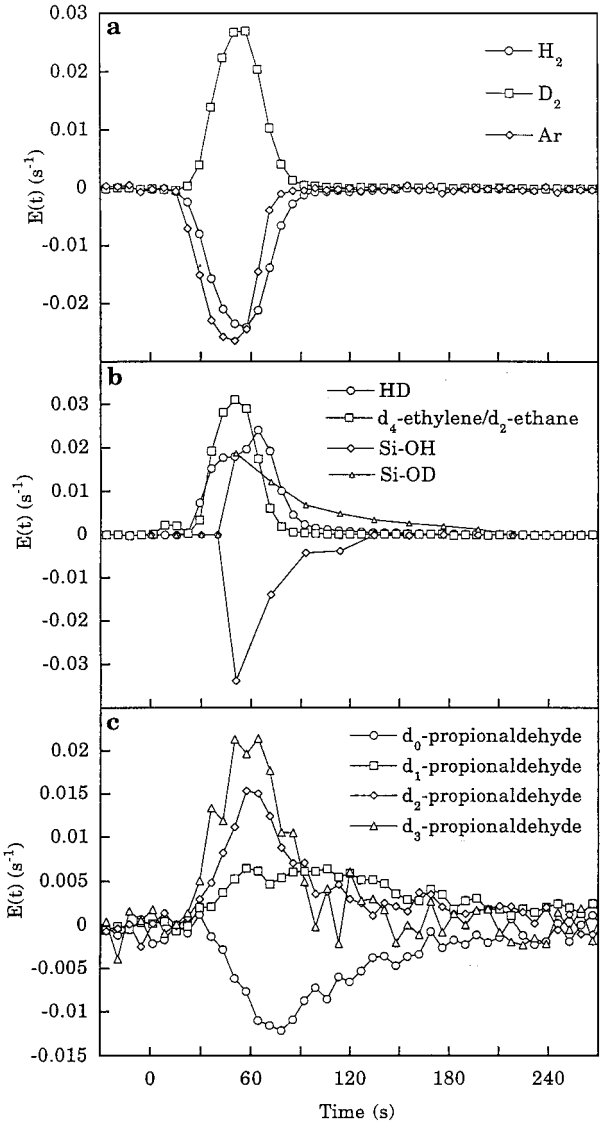

FIG. 2. Normalized product responses to a 10 cm^3 D_2 pulse into H_2 at 30 : 30 : 30 : 30 cm^3/min $H_2/CO/C_2H_4$/He.

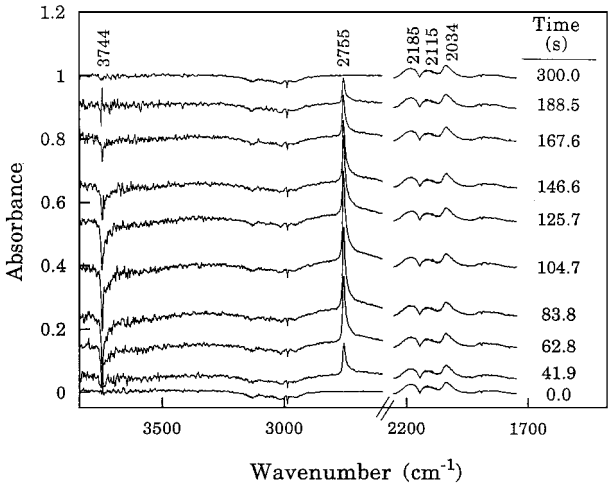

FIG. 3. *In situ* IR spectra during D_2 pulse transient at 30:30:30:30 cm^3/min $H_2/CO/C_2H_4$/He.

Figure 3 shows the IR spectra collected during the transient. Si–OH is represented by the peak at 3744 cm^{-1} while Si–OD is represented by the peak at 2755 cm^{-1}. Deuterium is nearly twice as heavy as hydrogen; as a result, Si–OD stretches at a lower frequecy than Si–OH. The area under each of these IR peaks, which corresponds to adsorbate concentration, was calculated and plotted versus time as an $E(t)$ curve in Fig. 2 along with the other response curves. The other prominent peaks from Fig. 3 are gas-phase CO, represented by the doublet at 2185 and 2115 cm^{-1}, and linear CO, represented by the peak at 2034 cm^{-1}. The IR spectra of these species were not affected by the D_2 pulses, indicating that the steady-state condition for adsorbed CO was not disturbed by the pulse D_2 transient.

One of the key features of Fig. 2a is the nearly symmetric H_2 and D_2 transients. This demonstrates that the total concentration of labeled plus nonlabeled isotope remains nearly constant. Another important feature is the lag in the H_2 response with respect to Ar, indicating the occurrence of reversible H_2 adsorption on the catalyst surface.

Figure 2b shows the Si–OH, Si–OD, HD, and d_4-ethylene/d_2-ethane transient responses. The delayed responses of Si–OH and Si–OD relative to those of H_2 and D_2 represent the time necessary for adsorbed H/D to migrate from the metal surface to the support. Also, the slower return to the baseline of Si–OD relative to Si–OH suggests the presence of an isotope effect on the surface. It should be noted that the majority (~98%) of Si–OD does not directly exchange with gaseous D_2 (20). An H_2/D_2 step switch experiment on SiO_2 and Mn–Rh/SiO_2 showed that the Si–OD intensity on SiO_2 is approximately 2% of that on Mn–Rh/SiO_2; the average residence time of Si–OD on SiO_2 is nearly ten times larger than that on Mn–Rh/SiO_2 (20). The formation of the two-hump HD response is due to the increase and decrease of D_2 and H_2 concentrations during the transient. The two local maxima, i.e., two peaks, exhibited by the HD response correspond to the points where the surface coverages of $^*H$ and $^*D$ are nearly equal. The typically larger second hump is due to an isotope effect. A more detailed account of the significance of the HD responses will be discussed later. Due to the overlapping of all deuterated ethane responses, only the d_2-ethane response in shown in Fig. 2b. The response of d_2-ethane closely followed that of D_2. There is no measurable difference in residence times between D_2 and the d_i-ethane responses, indicating the existence of a very rapid H/D exchange with the adsorbed ethyl within the intermediates pool. This is consistent with previous studies on the same Mn–Rh/SiO_2 catalyst (18, 20).

Figure 2c contains the deuterated propionaldehyde transient responses. The deuterated propionaldehyde species exhibit behavior consistent with previous studies (18, 20). The d_1- and d_2-propionaldehyde species give a two-hump response. Due to the smaller amount of d_2-propionaldehyde produced, the characteristics of the two-hump response is vague. The d_0- and d_3-propionaldehyde species, on the other hand, give a one-hump response. The d_3-propionaldehyde response, and especially those of higher deuterated products (not shown), are noisy relative to their less deuterated counterparts because smaller amounts of higher deuterated products are produced. The decay portion of the second-hump d_1-propionaldehyde responses is parallel to the decay of Si–OD as shown in Figs. 2b and 2c. The differences in the characteristics of the responses suggest that the formation of d_1-, d_2-, and d_3-propionaldehyde involves two different modes of deuteration which will be further illustrated in Fig. 11.

Since reactant partial pressure has a strong influence on product formation rate, it is reasonable to expect that it will also affect the transient responses. The most apparent changes occur with varying H_2 partial pressure. Because D_2 is pulsed into H_2, varying hydrogen partial pressures through altering of hydrogen flow rates has a direct impact on the H_2 and D_2 transient responses as shown in Fig. 4. These reactant responses, in turn, have a direct impact on the product responses as shown in Figs. 5 and 6, which depict Si–OH/Si–OD and d_i-propionaldehyde transients, respectively. The d_2-propionaldehyde response is not included in Fig. 6 for the sake of clarity in the figure and because it is not used for modeling. At low hydrogen partial pressures, D_2 was injected into a low H_2 flow rate stream and, as a result, the residence times of all species are large. At these low hydrogen partial pressures, the d_i-propionaldehyde responses are noisy due to their low formation rates and spread of a given amount of d_i-propionaldehyde in a long pulse period. Similar parallel decay for d_1-propionaldehyde and Si–OD in Fig. 2 has also been observed for the reaction under various reactant partial pressures as shown in Figs. 5 and 6, indicating that the decay portion of the d_1-propionaldehyde curve may result from the reaction with spillover deuterium

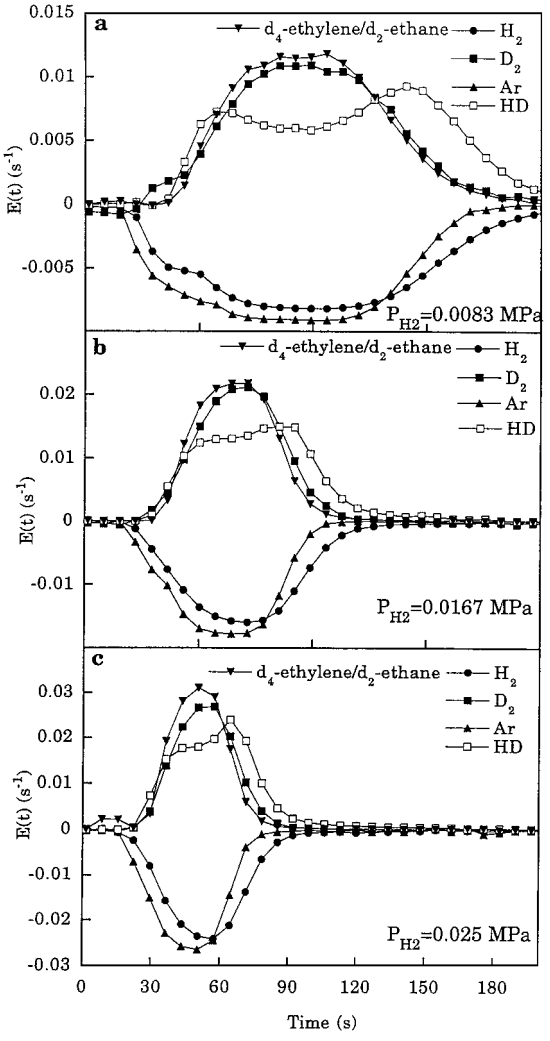

FIG. 4. Normalized d_2-ethane/d_4-ethylene, H_2, D_2, HD, and Ar responses to a D_2 pulse at hydrogen partial pressure of (a) 0.0083 MPa (10 cm^3/min), (b) 0.0167 MPa (20 cm^3/min), and (c) 0.025 MPa (30 cm^3/min).

from Si–OD. One important feature from Figs. 6b, 6c, and 6d is the rapid decay exhibited by the d_3-propionaldehyde response. This characteristic decay coupled with the slow decay of d_1-propionaldehyde will allow deconvolution of the two different modes of acyl deuteration.

The normalized responses, or $E(t)$ curves, can be used to calculate the average residence time, τ, of each species i from

$$\tau_i = \int_0^\infty t E_i(t)\, dt. \qquad [4]$$

τ_i allows quantification of the lead–lag relationship and can be used to determine the average residence times of intermediate species adsorbed on the catalyst surface. For example, the $E(t)$ curves for D_2 from Fig. 4 are a result of combined effects—transportation of D_2 from the pulsing loop to the MS ionization chamber, adsorption and desorption of D_2 on the catalyst surface, and its interaction with the walls of the transport lines and/or reactor vessel. As a result, τ_{*D}, the average residence time of adsorbed deuterium, must be determined from the equation

$$\tau_{*D} = \tau_{D_2} - \tau_{Ar} - \tau_{Dt}, \qquad [5]$$

where τ_{D_2} is the average residence time of the gaseous D_2

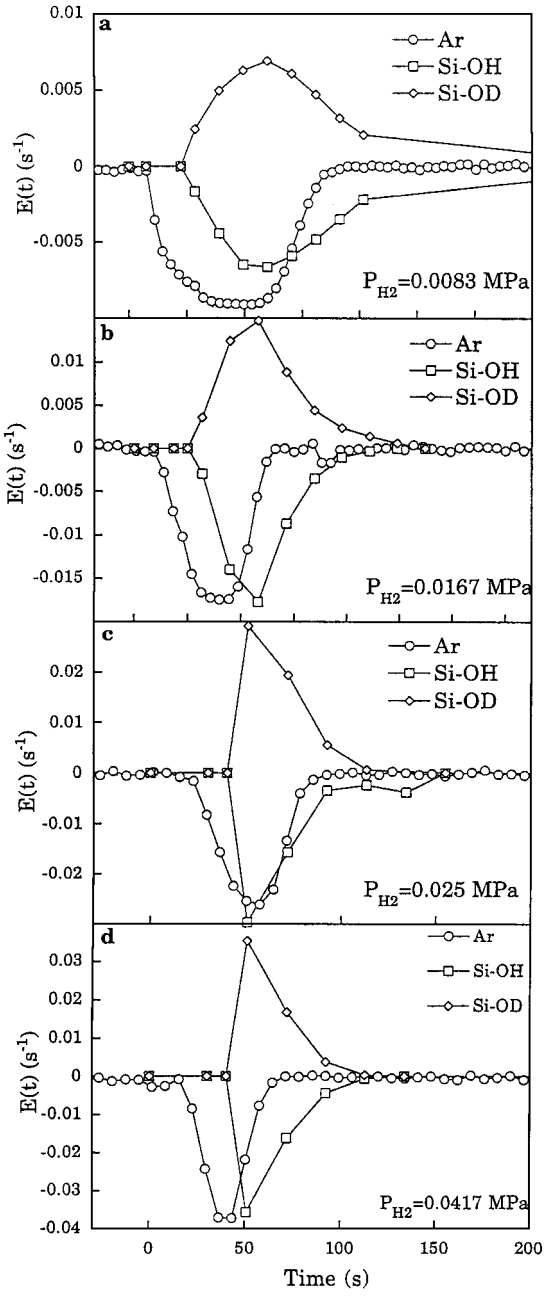

FIG. 5. Normalized Ar, Si–OH, and Si–OD responses to a D_2 pulse at hydrogen partial pressure of (a) 0.0083 MPa (10 cm^3/min), (b) 0.0167 MPa (20 cm^3/min), (c) 0.025 MPa (30 cm^3/min), and (d) 0.0417 MPa (50 cm^3/min).

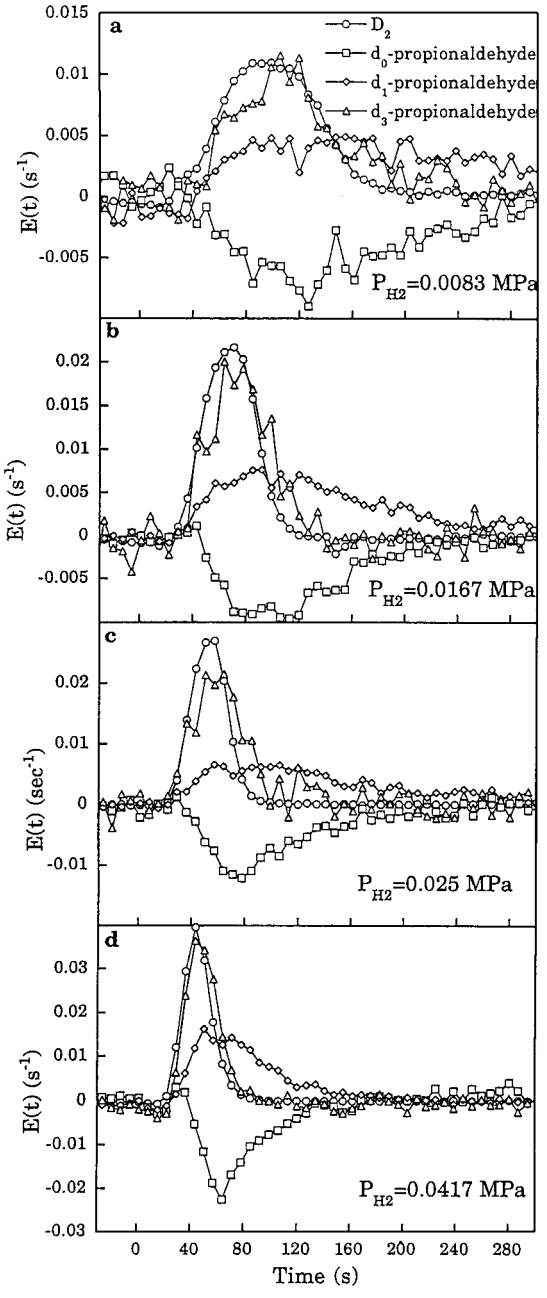

FIG. 6. Normalized d_i-propionaldehyde responses to a D_2 pulse at hydrogen partial pressure of (a) 0.0083 MPa (10 cm^3/min), (b) 0.0167 MPa (20 cm^3/min), (c) 0.025 MPa (30 cm^3/min), and (d) 0.0417 MPa (50 cm^3/min).

response measured by MS, τ_{Ar} is the average residence time of gaseous argon, and τ_{Dt} is the average residence time of D_2 interaction with the tubing/reactor walls. Since Ar is an inert tracer and does not interact with the catalyst or the tubing/reactor walls, its response describes exclusively the flow pattern within the reactor system. Thus, τ_{Ar} accounts for the residence time of D_2 in the gas phase, which travels from the pulsing loop to the MS. In order to ascertain the effects of the walls of the tubing and reactor system on D_2 without the catalyst present or, in other words, to quantify the τ_{Dt} term, a blank run was performed with SiO_2 in place of Mn–Rh/SiO_2 in which D_2 was stepped into H_2 for the $H_2/CO/C_2H_4$/He reaction. Again, Ar was present in the H_2 stream and the volumetric flow rates of each reactant were equal to 30 cm^3/min. Interestingly, a visible difference between D_2 and Ar residence times was detected. Quantitatively, this difference was

$$\tau_{Dt} = \tau_{D_2} - \tau_{Ar} = 2.1 \text{ s}. \quad [6]$$

Physically, τ_{Dt} signifies interaction between the D_2 and the walls of the reactor and tubing and must be accounted for in all τ_{*D} calculations. However, since blank runs are not available for hydrogen flow rates of 10, 20, and 50 cm^3/min, this correction factor will be adjusted for these runs accordingly assuming an inverse proportional relationship between the correction factor and flow rate.

τ_{*D} as a function of reactant partial pressure was determined and plotted in Fig. 7. The average residence times of other important species, Si–OD and d_i-propionaldehyde, were also determined as a function of reactant partial pressure and plotted in Figs. 8 and 9, respectively. The average residence time of Si–OD, which reflects the time for conversion of *D to Si–OD, was determined using a modified version of Eq. [4],

$$\tau_i = \int_0^\infty t E_i(t)\, dt - \tau_{Ar}, \quad [7]$$

where i, in this case, is Si–OD. In order for a fair comparison, τ_{Ar} must be subtracted from the quantity $\int_0^\infty t E_{Si\text{-}OD}(t)\, dt$ for the same reasons outlined above for Eq. [5]. τ_{Ar} accounts for the transportation lag due to gaseous species since D_2 travels with Ar in the same flow pattern to arrive on the catalyst surface. The resultant residence time will be

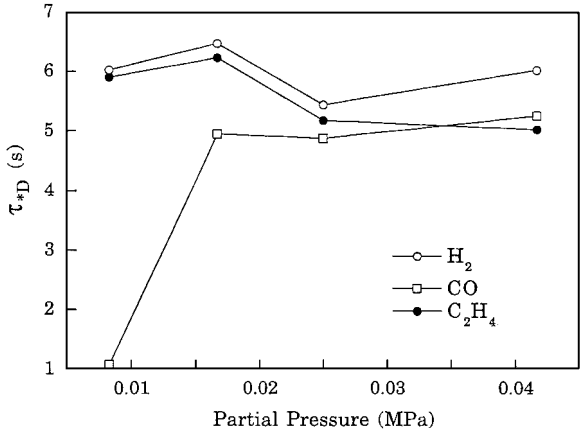

FIG. 7. Average residence time of *D versus reactant partial pressure. (When partial pressure of a reactant is varied, the remaining two reactants stay constant at 0.025 MPa.)

slightly underestimated in comparison to gas-phase products; in other words, Si–OD did not traverse the pipe from the reactor to the MS as Ar was required to do. Because the residence times are underestimated and are also relatively large compared to τ_{Dt}, it is not necessary to subtract the τ_{Dt} factor from Eq. [7]. The d_0- and d_1-propionaldehyde residence times are nearly equal and are also greater than both d_2- and d_3-propionaldehyde residence times.

Participation of Si–OD in d_1-Propionaldehyde Formation

The role of Si–OD in product formation may be unraveled by comparing the Si–OD response with those of deuterated ethane and propionaldehyde in Figs. 2 and 4–6. The Si–OD response lagged behind those of deuterated ethane and d_3-propionaldehyde, indicating that the formation of these deuterated products did not involve Si–OD. The source of deuterium for the formation of these products appears to be adsorbed deuterium on the Rh surface. In contrast, the decay of the Si–OD curve closely followed that of the d_1-propionaldehye curve, suggesting participation of Si–OD in d_1-propionaldehyde formation.

To verify the above suggestion, we have first exposed the catalyst to D_2 at 298 K and then isolated deuterium on SiO_2 (i.e., Si–OD) by reacting away the metal-adsorbed deuterium with ethylene. Figure 10b shows that exposure of the catalyst to D_2 produced Si–OD. Subsequent exposure of the catalyst to ethylene produced deuterated ethane with little variation in the Si–OD intensity, indicating that Si–OD is not accessible to adsorbed ethylene on the Rh surface for deuteration (i.e., hydrogenation). The Si–OD intensity, plotted versus time in Fig. 10a, began decreasing upon the addition of the $CO/H_2/C_2H_4$ reactant mixture entering the reactor. Interestingly, the d_1-propionaldehyde profile followed closely that of Si–OD. The only deuterated product observed is d_1-propionaldehyde, confirming the postulated role of Si–OD in d_1-propionaldehyde formation.

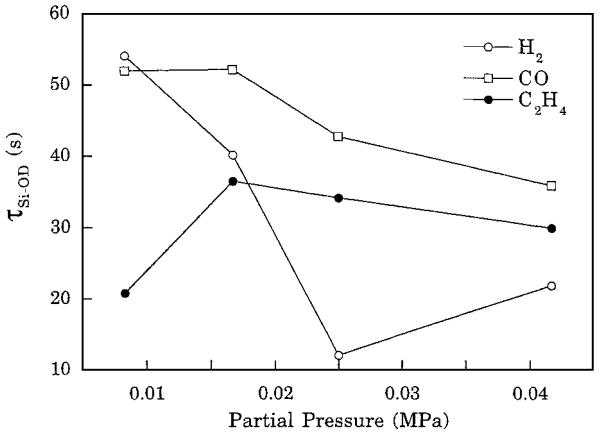

FIG. 8. Average residence time of Si–OD versus reactant partial pressure.

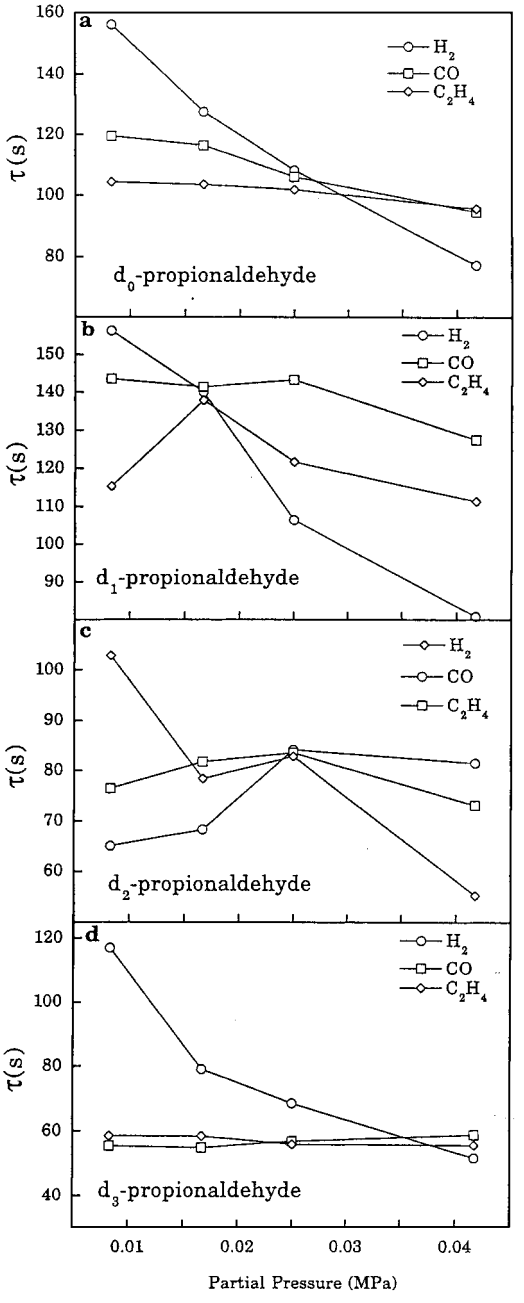

FIG. 9. Average residence time of (a) d_0-propionaldehyde, (b) d_1-propionaldehyde, (c) d_2-propionaldehyde, and (d) d_3-propionaldehyde versus reactant partial pressure.

DISCUSSION

Model Development

The transient responses of the reaction system carry mechanistic information. To elucidate the mechanistic parameters from transient responses, compartment models which describe the reaction must be generated. These compartment models are, in turn, derived from a proposed

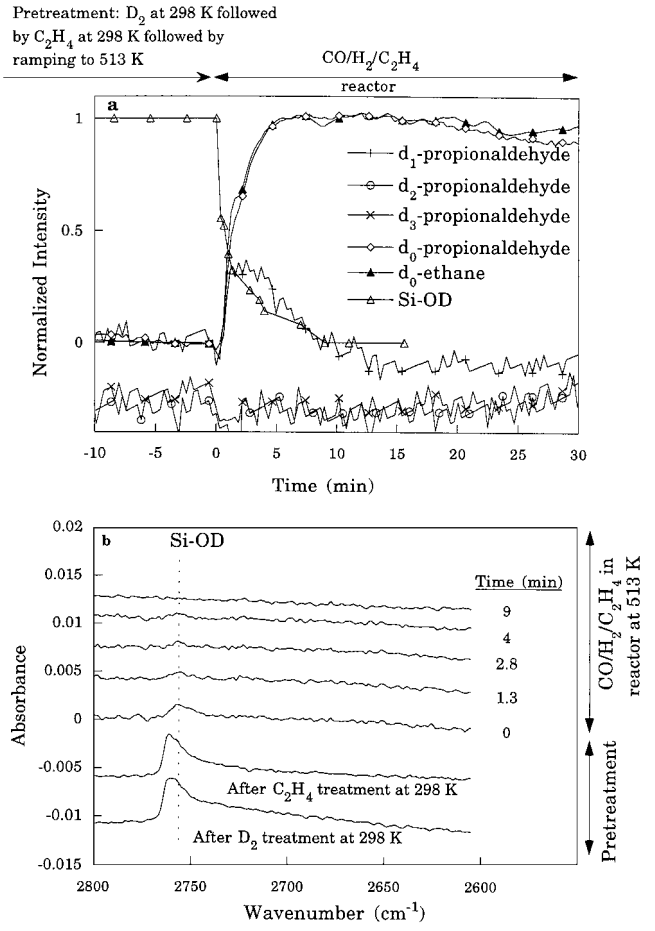

FIG. 10. Incorporation of Si–OD in d_1-propionaldehyde formation at 513 K: (a) product and Si–OD profiles and (b) transient Si–OD infrared spectra.

reaction mechanism. The proposed pathway for ethane and propionaldehyde formation utilized in this study and the resultant compartment models are shown in Fig. 11. Corresponding variables are defined in Table 1. Responses of deuterium-containing products to the D_2 pulse allows tracing of the deuterium/hydrogen pathway in the depicted reaction pathway. Hydrogen first undergoes reversible adsorption. Subsequently, adsorbed hydrogen may (i) spillover to the SiO_2 surface to form Si–OH, (ii) hydrogenate adsorbed ethylene to form an adsorbed ethyl species, (iii) hydrogenate adsorbed ethyl to produce ethane, or (iv) hydrogenate adsorbed acyl to form propionaldehyde. In addition, Si–OH serves as a hydrogen source for hydrogenation of adsorbed acyl. The inability of Si–OH to hydrogenate ethylene and lack of HD formation upon exposure of Si–OD to $CO/H_2/C_2H_4$ in Figs. 10a and 10b suggest the dominant reaction pathway for Si–OD is deuteration (i.e., hydrogenation) of adsorbed acyl species. It should also be noted that adsorbed ethylene, ethyl, and acyl can undergo rapid exchange with adsorbed hydrogen on the metal surface (12, 13, 20, 22, 23). In other words, hydrogen atoms on these species are able to exchange with metal chemisorbed hydrogen atoms. The selectivity toward ethane or propionaldehyde depends on the reactivity of adsorbed ethyl species toward hydrogenation or CO insertion. Participation of adsorbed ethyl in both hydrogenation and CO insertion is supported by the similarity in reaction order with respect to C_2H_4 for ethane and propionaldehyde formation. A number of previous studies have supported the validity of this overall mechanistic scheme (17–20).

There are many possible models on which to base kinetic analyses; these models are discussed in detail in previous work (24). The models depicted in Fig. 11 are derived from the hydrogen pathway. It is assumed that all species in each pool, i.e., compartment, react homogeneously with the same reactivity and that the species in each pool reacts independent of the others. Model 1 describes the pathway for conversion of H_2/D_2 to $C_2H_xD_{6-x}$ via (i) the pool of $^*H/^*D$ and (ii) the pool of adsorbed ethyl, $^*C_2H_xD_{5-x}$. Model 2

TABLE 1

Variable Definitions and Units for Fig. 11 and Table 2

υ_{+1}	Rate of hydrogen adsorption (s^{-1})
υ_{-1}	Rate of hydrogen desorption (s^{-1})
$\theta_{*\mathrm{eth}}$	Ethane pool intermediate surface coverage
k_{eth}	Rate coefficient for hydrogenation of ethane pool intermediates (s^{-1})
τ_{eth}	Ethane pool residence time (s)
$\theta_{*\mathrm{H}}$	Model 2/Model 3, pool 1 intermediate surface coverage, or hydrogen surface coverage.
$\theta_{*\mathrm{acyl\,1}}$	Model 2, pool 2 intermediate surface coverage
k_{H}	Rate coefficient for CO insertion into Model 2/ Model 3, pool 1 intermediates (s^{-1})
$k_{\mathrm{acyl\,1}}$	Rate coefficient for hydrogenation of Model 2, pool 2 intermediates (s^{-1})
k_{acyl1}	Elementary rate constant for hydrogenation of adsorbed acyl via metal-chemisorbed hydrogen (s^{-1})
τ_{H}	Model 2/Model 3, pool 1 residence time (s^{-1}); $\tau_{\mathrm{H}} = \tau_{^*\mathrm{D}} = \tau_{\mathrm{D_2}}$
$\tau_{\mathrm{acyl\,1}}$	Model 2, pool 2 residence time (s^{-1})
$\theta_{*\mathrm{acyl\,2}}$	Model 3, pool 2 intermediate surface coverage
$k_{\mathrm{acyl\,2}}$	Rate coefficient for hydrogenation of Model 3, pool 2 intermediates (s^{-1})
k_{acyl2}	Elementary rate constant for hydrogenation of adsorbed acyl via spillover hydrogen (s^{-1})
$\tau_{\mathrm{acyl\,2}}$	Model 3, pool 2 residence time (s^{-1})
$\theta_{\mathrm{Si\text{-}OH}}$	Coverage of spillover hydrogen
$\mathrm{TOF}_{\mathrm{ethane}}$	Rate of ethane production (s^{-1})
$\mathrm{TOF}_{^*\mathrm{C_2H_xD_{5-x}CO}}$	Rate of production of adsorbed acyl: Model 2/ Model 3, pool 2 (s^{-1})
$\mathrm{TOF}^{\mathrm{M\text{-}D}}_{\mathrm{propionaldehyde}}$	Rate of propionaldehyde production via Model 2 pathway with adsorbed deuterium on metal (s^{-1})
$\mathrm{TOF}^{\mathrm{Si\text{-}OD}}_{\mathrm{propionaldehyde}}$	Rate of propionaldehyde production via Model 3 pathway with Si–OD (s^{-1})

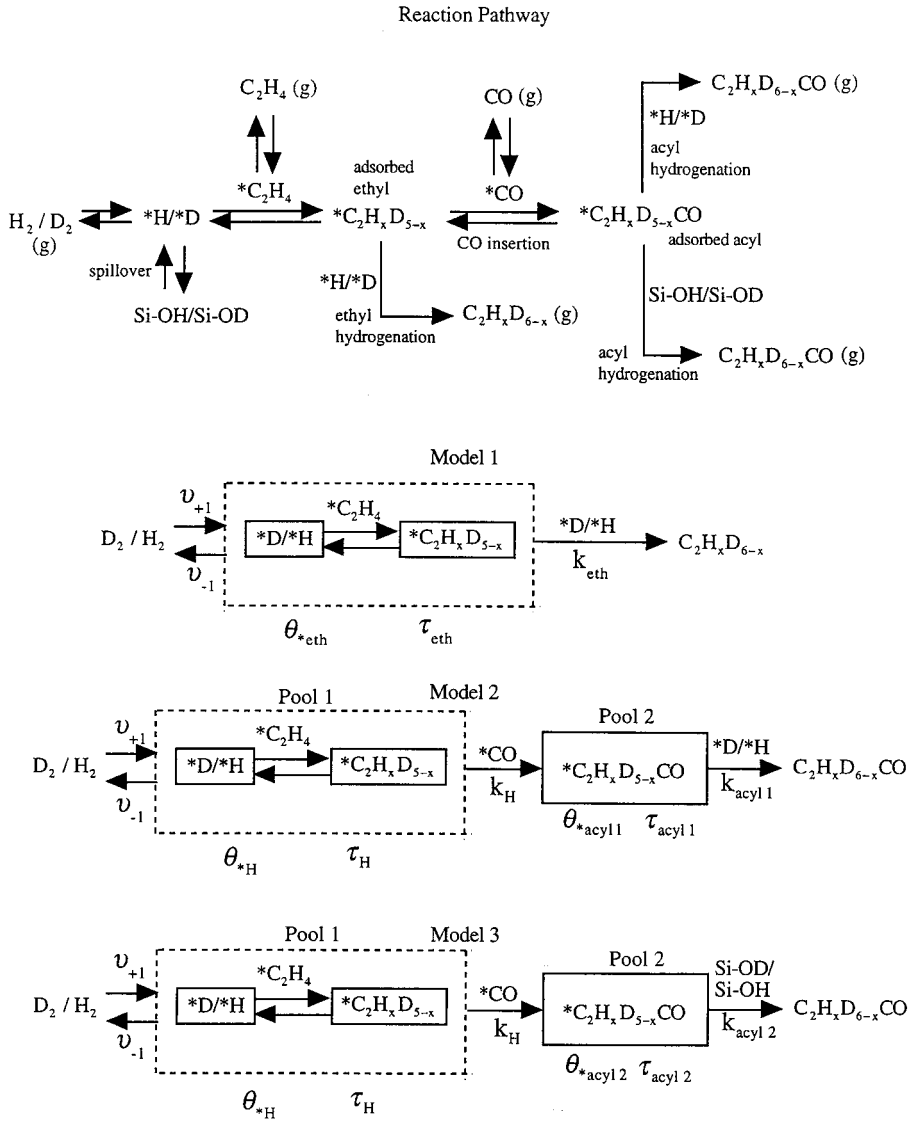

FIG. 11. Ethylene hydroformylation reaction pathway and resultant ethane and propionaldehyde compartment models. (* denotes an adsorbed species.)

describes the conversion of H_2/D_2 to $C_2H_xD_{6-x}CO$ via three intermediate pools, $^*D/^*H$, $^*C_2H_xD_{5-x}$, and $^*C_2H_xD_{5-x}CO$. Model 3 is identical to Model 2 except for the acyl hydrogenation pathway. Model 2 suggests hydrogenation of acyl by hydrogen chemisorbed on the metal and Model 3 by Si–OH, spillover hydrogen. These two models indicate that acyl is hydrogenated in parallel pathways with H–M and Si–OH. Both the $^*D/^*H$ and $^*C_2H_5D_{5-x}$ pools may be lumped into a single intermediates pool for all the models because of (i) the rapid reversible reaction between $^*D/^*H$ and $^*C_2H_xD_{5-x}$ and (ii) the low values of ethyl surface coverage as determined in previous studies ($\theta < 0.03$) (18, 25). These single pools are designated by a dashed line. Coverages of these pools are denoted by θ_{*eth} in Model 1 and θ_{*H} in Models 2 and 3.

Determination of Model Parameters

The equations in Table 2 used to determine the values of the reaction parameters for the models depicted in Fig. 11 were previously derived by mole balances of the pools-in-series model and the assumption that the rate of transfer for the deuterium-containing species from one pool to the subsequent pool is proportional to the coverage of intermediates (24). As a result, this rate of transfer, or TOF_i, can be described as follows:

$$TOF_i = k_j\theta_{*j}, \quad [8]$$

where i is the species being produced, k_j is the rate coefficient, or proportionality constant, of the product precursor from pool j, and θ_{*j} is the coverage of precursors, i.e.,

TABLE 2

Equations which Describe the Compartment Models Depicted in Fig. 11

Model	Model equations		Elementary rate equations	
1	$\mathrm{TOF}_{\mathrm{ethane}} = \mathrm{k}_{\mathrm{eth}}\theta_{*\mathrm{eth}}$	[9]		
	$\mathrm{TOF}_{\mathrm{ethane}} = \dfrac{\theta_{*\mathrm{eth}}}{\tau_{\mathrm{eth}}\left(1 + \frac{\upsilon_{-1}}{\mathrm{TOF}_{\mathrm{ethane}}}\right)}$	[10]		
2	$\theta_{*\mathrm{H}} = \tau_{\mathrm{H}}\upsilon_{+1}$	[11]		
	$\mathrm{TOF}_{*\mathrm{C_2H_xD_{5-x}CO}} = \mathrm{k}_{\mathrm{H}}\theta_{*\mathrm{H}}$	[12]		
	$\mathrm{TOF}_{*\mathrm{C_2H_xD_{5-x}CO}} = \dfrac{\theta_{*\mathrm{H}}}{\tau_{\mathrm{H}}\left(1 + \frac{\upsilon_{-1}}{\mathrm{TOF}_{\mathrm{ethane}}}\right)}$	[13]		
	$\mathrm{TOF}^{\text{M-D}}_{\text{propionaldehyde}} = \mathrm{k}_{\mathrm{acyl\,1}}\theta_{*\mathrm{acyl\,1}}$	[14]	$\mathrm{TOF}^{\text{M-D}}_{\text{propionaldehyde}} = k_{acyl\,1}\theta_{*\mathrm{acyl\,1}}\theta_{*\mathrm{H}}$	[15]
	$\mathrm{TOF}^{\text{M-D}}_{\text{propionaldehyde}} = \frac{\theta_{*\mathrm{acyl\,1}}}{\tau_{\mathrm{acyl\,1}}} = \frac{\theta_{*\mathrm{acyl\,1}}}{\tau_{\mathrm{d_3\text{-propionaldehyde}}} - \tau_{\mathrm{D_2}}}$	[17]	$\mathrm{k}_{\mathrm{acyl\,1}} = k_{acyl\,1}\theta_{*\mathrm{H}}$	[16]
3	$\mathrm{TOF}^{\text{Si-OD}}_{\text{propionaldehyde}} = \mathrm{k}_{\mathrm{acyl\,2}}\theta_{*\mathrm{acyl\,2}}$	[18]	$\mathrm{TOF}^{\text{Si-OD}}_{\text{propionaldehyde}} = k_{acyl\,2}\theta_{*\mathrm{acyl\,2}}\theta_{\text{Si-OH}}$	[19]
	$\mathrm{TOF}^{\text{Si-OD}}_{\text{propionaldehyde}} = \frac{\theta_{*\mathrm{acyl\,2}}}{\tau_{\mathrm{acyl\,2}}} = \frac{\theta_{*\mathrm{acyl\,2}}}{\tau_{\mathrm{d_1\text{-propionaldehyde}}} - \tau_{\mathrm{d_3\text{-propionaldehyde}}}}$	[21]		[20]

intermediates, from pool j. The rate coefficient $\mathrm{k_j}$ reflects the activity of pool j intermediates. For instance, under steady-state reaction conditions, the rate of propionaldehyde formation in Model 2 can be described by

$$\mathrm{TOF}^{\text{M-D}}_{\text{propionaldehyde}} = \mathrm{k}_{\mathrm{acyl\,1}}\theta_{*\mathrm{acyl\,1}}. \quad [14]$$

The rate of propionaldehyde formation, which involves the reaction of adsorbed acyl with metal-chemisorbed hydrogen, can also be expressed by the elementary rate law

$$\mathrm{TOF}^{\text{M-D}}_{\text{propionaldehyde}} = k_{acyl\,1}\theta_{*\mathrm{acyl\,1}}\theta_{*\mathrm{H}}, \quad [15]$$

where $k_{acyl\,1}$ is an elementary rate constant. Equating Eqs. [14] and [15] yields

$$\mathrm{k}_{\mathrm{acyl\,1}} = k_{acyl\,1}\theta_{*\mathrm{H}}, \quad [16]$$

revealing that $\mathrm{k}_{\mathrm{acyl\,1}}$ is indeed a pseudo-first-order rate constant. Similar relationships for the rate parameters and the elementary rate constants were obtained for Model 3 in Table 2. However, analogous derivations cannot be done for the first pools of each of the models because the $^*\mathrm{D}/^*\mathrm{H}$ and $^*\mathrm{C_2H_xD_{5-x}}$ pools cannot be decoupled. Thus, elementary rate constants for ethyl hydrogenation and CO insertion cannot be determined. Also, the coverage of Si–OH is unavailable for finding $k_{acyl\,2}$ in Eq. [19]; only $k_{acyl\,1}$ can be solved.

Accurate interpretation of the physical significance of the $\mathrm{d_i}$-propionaldehyde responses is important for understanding how the models in Fig. 11 and equations in Table 2 were developed. The two-hump $\mathrm{d_1}$- and $\mathrm{d_2}$-propionaldehyde responses in Figs. 2 and 6 consist of three portions: the first hump, the second hump, and the decay portion of the second hump. These are the result of differing reaction pathways. For instance, the first hump of the $\mathrm{d_1}$- and $\mathrm{d_2}$-propionaldehyde species was due to rapid H/D exchange, possibly through keto-enol tautomerism, followed by hydrogenation/deuteration of adsorbed acyl with adsorbed deuterium/hydrogen (20, 26). The rapid rise of the initial humps also supports this suggestion. The second hump is the result of deuterium which has traveled through the entire mechanistic path shown in Fig. 11:

$$\mathrm{H_2/D_2\ (g)} \leftrightarrow {}^*\mathrm{H}/{}^*\mathrm{D} \overset{^*\mathrm{C_2H_4}}{\longleftrightarrow} {}^*\mathrm{C_2H_xD_{5-x}}$$
$$\overset{^*\mathrm{CO}}{\longleftrightarrow} {}^*\mathrm{C_2H_xD_{5-x}CO} \overset{^*\mathrm{H}/^*\mathrm{D}}{\longleftrightarrow} {}^*\mathrm{C_2H_xD_{6-x}CO\ (g)}.$$

This is supported by a previous study that utilized $^{13}\mathrm{CO}$ tracer; the $\mathrm{C_2H_5{}^{13}CHO}$ response peak corresponds closely with the second hump of the $\mathrm{d_i}$-propionaldehyde response (18). Finally, the slow decay of the second hump is parallel with the Si–OD response due to deuteration of adsorbed $\mathrm{C_2H_5CO}$ by spillover deuterium. The absence of a second hump for $\mathrm{d_3}$-propionaldehyde could be due to a low rate of formation of the deuterated propionaldehyde isomers resulting from hydrogen/deuterium traveling through the entire reaction pathway.

As previously discussed, the $\mathrm{d_3}$-propionaldehyde response does not exhibit the slow decay response as do the other propionaldehyde products. Therefore, it is assumed that this particular response represents exclusively hydrogenation/deuteration of the adsorbed acyl species with metal chemisorbed hydrogen/deuterium. Thus, the residence time of this species is the most logical choice for inclusion in Eq. [17], which is used to characterize the second pool of Model 2, acyl hydrogenated by metal-chemisorbed hydrogen. The decay portion of the $\mathrm{d_1}$-propionaldehyde species is assumed to best represent deuteration via spillover deuterium (Si–OD). Thus, the $\mathrm{d_1}$-propionaldehyde response is the result of two modes of deuteration: metal chemisorbed deuterium and spillover deuterium.

The difference between the d_1-propionaldehyde and d_3-propionaldehyde average residence times, $\tau_{d_1\text{-propionaldehyde}} - \tau_{d_3\text{-propionaldehyde}}$ in Eq. [21], represents the residence time of product resulting primarily from spillover hydrogen. This quantity is $\tau_{acyl\,2}$.

It is important to note that $TOF^{M\text{-}D}_{propionaldehyde}$ and $TOF^{Si\text{-}OD}_{propionaldehyde}$ in Models 2 and 3 used for the calculation of $\theta_{*acyl\,1}$ and $\theta_{*acyl\,2}$ (Eqs. [14] and [18], respectively) is not the total rate of propionaldehyde formation, but is the fraction of the total attributable to each mode of acyl hydrogenation. In order to estimate this fraction, the area under the decay portion of the d_1-propionaldehyde response, which represents acyl hydrogenated via spillover hydrogen, was ratioed to the area under the entire curve, which represents both modes of acyl hydrogenation. This ratio was found to be approximately 0.5 for all runs. Thus, $TOF_{propionaldehyde}$ in Eqs. [14] and [18] is assumed to be one half the steady-state values reported in Fig. 1.

The equations from Table 2 provide the relationship between the rate of hydrogen adsorption–desorption, average residence times and coverages of adsorbed intermediates in the compartment model pools, and rate of product formation. The rates of product formation, i.e., TOF_{ethane} and $TOF_{propionaldehyde}$, were determined by GC and MS analysis of the reactor effluent. The average residence times, τ_{eth}, τ_H, $\tau_{acyl\,1}$, and $\tau_{acyl\,2}$, were determined by the transient responses of reactants and products. Table 3a lists all the experimentally determined quantities. No reliable approach, however, has been developed for the measurement of the rate of hydrogen adsorption, υ_{+1}, and desorption, υ_{-1}, under reaction conditions. Often, an assumption is made that all the entering tracer, in this case D_2, adsorbs on the catalyst surface because of the difficulty in obtaining actual values for these rates (24). Subsequent to adsorption, the tracer either desorbs or reacts to form products:

$$\upsilon_{+1} = \upsilon_{-1} + TOF_{products}. \quad [22]$$

However, in many cases, the assumption that 100%, i.e., all, of the hydrogen entering the reactor adsorbs on the catalyst surface is invalid, especially when the experiment is performed with a differential reactor, as is the case in this study. There is often a substantial amount of bypass involved, which would lead to inaccurate values for these rates and hence inaccurate values for the model pool parameters.

TABLE 3a

Experimentally Determined Quantities

Parameter	Method
υ_{-1}	Transient HD response; $\upsilon_{-1} = 3r_{HD}$ [24]
τ_{eth}, τ_{D2}, τ_H, $\tau_{d1\text{-propionaldehyde}}$, $\tau_{d3\text{-propionaldehyde}}$	Transient response of species i; $\tau_i = \int_0^\infty tE_i(t)\,dt - \tau_{Ar}$ [7]
$TOF^{M\text{-}D}_{propionaldehyde}$	Transient d_1-propionaldehyde response; area fraction under curve corresponding to deuteration via metal-chemisorbed D.
$TOF^{Si\text{-}OD}_{propionaldehyde}$	Transient d_1-propionaldehyde response; area fraction under curve corresponding to deuteration via spillover D.
TOF_{ethane}, $TOF_{propionaldehyde}$, $TOF_{products} = TOF_{eathane} + TOF_{propionaldehyde}$	Rate determination by GC analysis and flow rate.

Determination of Rate of Hydrogen Desorption

To accurately estimate values for the steady-state rates of hydrogen adsorption and desorption, a new method has been developed. The key to this new method lies in the ability to evaluate the HD pulse response. The HD transient response is a result of the reaction of adsorbed hydrogen and deuterium. The rate of HD formation, r_{HD}, depends on θ_{*H} and θ_{*D}, which should be proportional to the H_2 and D_2 transient. Figure 12a provides the hypothetical variation of θ_{*H} and θ_{*D} during a D_2 into H_2 pulse to illustrate the physical significance of the two-hump HD response. Assuming the rate of HD formation follows elementary reaction kinetics where

$$r_{HD} = k\theta_{*H}\theta_{*D} \quad [23]$$

and the surface reaction is rate limiting, variation of r_{HD} with changing θ_{*H} and θ_{*D} can be obtained and is shown in Fig. 12b. The symmetrical increase and decrease of θ_{*H} and θ_{*D} gives a two-hump response, each hump of equal size. The peaks of these humps, i.e., local maxima, occur at $\theta_{*H} = \theta_{*D} = \frac{1}{2}\theta_{*H}|_{SS}$, where $\theta_{*H}|_{SS}$ is the steady-state hydrogen surface coverage. However, if θ_{*D} lags the θ_{*H} response as shown in Fig. 12c, the resultant r_{HD} profile would consist of a small hump followed by a large hump. These two unequal-sized peaks were indeed observed in all of our D_2 pulse studies, three of which are shown in Fig. 4.

The area ratio of the two unequal r_{HD} humps, which results from θ_{*D} lagging θ_{*H}, signifies the H/D isotope effect. Neglecting this effect and assuming equal probability of forming H_2, D_2, and HD by associative desorption at $\theta_{*H} = \theta_{*D}$ lead to the conclusion that $r_{HD} = r_{H_2} = r_{D_2}$ at the maxima, i.e., peaks. Therefore, the total rate of $H_2/D_2/HD$ desorption, i.e., υ_{-1}, the steady-state rate of hydrogen desorption, is equal to $3r_{HD}$:

$$\upsilon_{-1} = 3r_{HD}. \quad [24]$$

r_{HD} can be estimated from the HD response with use of a calibration factor which converts the HD MS response to an HD rate curve. A detailed mathematical description for this procedure is shown elsewhere (27). To obtain a reasonable estimate of r_{HD} from two unequal hump responses, the

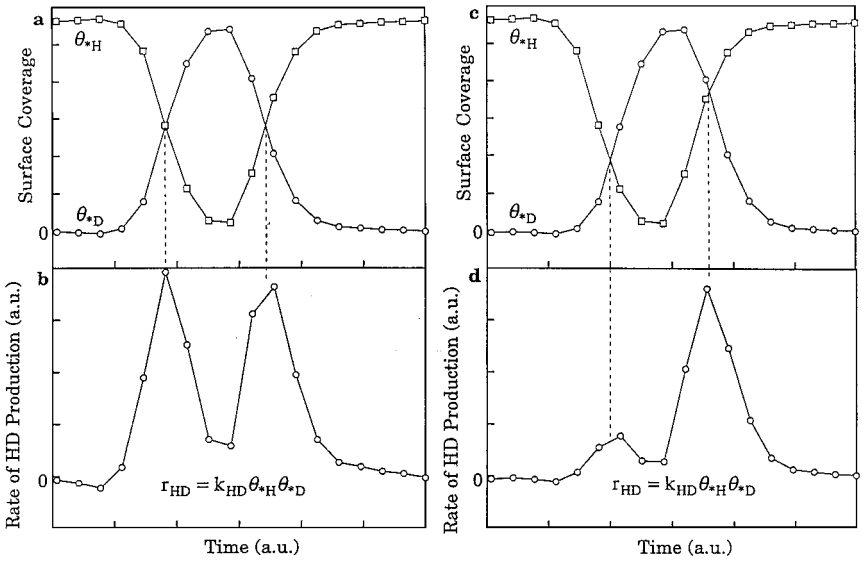

FIG. 12. (a) Illustration of the theoretical θ_{*H} (t) and θ_{*D} (t) profiles and (b) the resultant $r_{HD(t)}$ transient two-hump response used for υ_{-1} estimation. (c) and (d) are the result of θ_{*H} leading θ_{*D}.

average value,

$$\bar{r}_{HD} = \frac{r_{HD}|_{\text{local max 1}} + r_{HD}|_{\text{local max 2}}}{2}, \qquad [25]$$

is used in Eq. [24]. Once this value is obtained, the steady-state rate of hydrogen adsorption, υ_{+1}, can be obtained from Eq. [22]. The steady-state rates of hydrogen adsorption and desorption as a function of reactant partial pressure are shown in Fig. 13.

In order to check the validity of the calculated rate of desorption, a theoretical rate of desorption was estimated by transition-state theory (TST). This method necessitates knowledge of the partition functions of adsorbates and activated complexes as well as the activation energy of the elementary steps. These quantities are difficult to calculate, but there are some very useful guidelines in the literature that will be applied here (28). The elementary rate constant for associative hydrogen desorption, k_{H_2}, can be calculated as

$$k_{H_2} = \frac{k_b T}{h} \times \frac{Q^{\ddagger}_{H_2}}{(Q_{*H})^2} \times \exp\frac{-E_a}{RT} \times \frac{\text{sites}}{\text{area}}, \qquad [26]$$

where k_b is Bolzmann's constant, h is Plank's constant, T is temperature in K, $Q^{\ddagger}_{H_2}$ is the molecular partition function of the activated complex per unit area, Q_{*H} is the molecular partition function of adsorbed hydrogen per unit area, E_a is the activation energy, and R is the gas constant. The factor sites/area is a factor that arises from the conversion of an expression using rate and surface concentration to an expression that uses TOF and surface coverage. The value of this quantity is 3.92E13 cm^{-2} based on a support area of 350 m^2/g and H_2 chemisorption of 114 μmol/g for Mn–Rh/SiO_2. $Q^{\ddagger}_{H_2}$ is assumed to be a mobile species with no

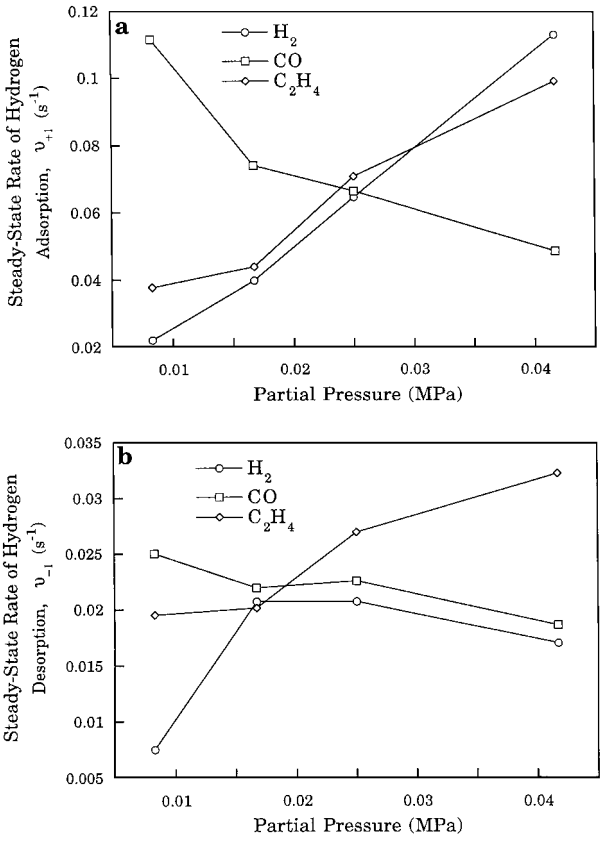

FIG. 13. (a) Rate of hydrogen adsorption and (b) hydrogen desorption versus reactant partial pressure.

rotational freedom and Q_{*H} a mobile species with one degree of rotational freedom, yielding values of 2.5E17 and 2.5E18 cm^{-2}, respectively. Assuming a Rh–H bond energy, $E_{Rh\text{-}H}$, of approximately 256 kJ/mol (29) and a H–H bond energy, $E_{H\text{-}H}$, of 431.4 kJ/mol, the activation energy, E_a, for associative H_2 desorption is 80.6 kJ/mol by

$$E_a = 2E_{Rh\text{-}H} - E_{H\text{-}H}. \quad [27]$$

This procedure for calculating the activation energy is described fully by Bell and co-workers (30). Plugging these values into Eq. [26] yields $k_{H_2} = 0.10\ s^{-1}$.

The experimental rate constant of hydrogen desorption, $k_{H_2,exp}$, must be determined from the actual rate of hydrogen desorption, υ_{-1}:

$$k_{H_2,exp} = \frac{\upsilon_{-1}}{\theta_{*H}^2} \quad [28]$$

Thus, values of θ_{*H} must be known in order to determine the rate constant. The value for θ_{*H} can be estimated by Eq. 11 in Table 2. An average value of 0.35 will be assigned to θ_{*H} and an average value of 0.02 s^{-1} to υ_{-1} will be used for comparison purposes. This yields $k_{H_2,exp} = 0.16\ s^{-1}$. This is in remarkable agreement with the theoretical k_{H_2} value of 0.10 s^{-1}, lending strong support to the validity of the assumptions. Thus, it is reasonable to use υ_{-1} for the calculation of model parameters as discussed in detail in a subsequent section.

Dependence of Model Parameters on Reactant Partial Pressure

Figure 13 shows that the rate of hydrogen adsorption decreases slightly with increasing P_{CO}, confirming that (a) H_2 and CO adsorb on the same sites and that (b) CO adsorbs more favorably than H_2 in a competitive environment, a phenomena reported in the literature (31, 32). As expected, the rate of hydrogen adsorption increases as H_2 partial pressure increases, which, of course, is consistent with the fact that the rate of dissociative adsorption is proportional to the product of the H_2 partial pressure and the number of vacant sites, θ_*, squared: $\upsilon_{+1} = kP_{H_2}\theta_*^2$. The rate is still increasing even at a H_2 partial pressure of 0.0417 MPa, which suggests that the pressure term is still dominating the θ_*^2 term, which should be decreasing with increasing H_2 partial pressure. Interestingly, the rate of hydrogen adsorption also increases in a similar fashion with increasing ethylene partial pressure. This indicates a favorable interaction between adsorbed hydrogen and adsorbed ethylene. This promotion effect is significant enough to dominate the effect of decreasing vacant sites.

Examining now the steady-state rates of hydrogen desorption versus partial pressure, these rates do not change appreciably with changing reactant partial pressure, with exception to an initial jump in rate as P_{H_2} changes from 0.0083 to 0.0167 MPa. Thus, increasing rates of hydrogen adsorption are reflected in product TOF rather than increases in desorption. (See Eq. [22].)

These rates, υ_{-1}, and the other experimentally measurable quantities, can now be used to solve for θ_{*eth}, k_{eth}, θ_{*H}, k_H, $\theta_{*acyl\,1}$, $k_{acyl\,1}$, $\theta_{*acyl\,2}$, and $k_{acyl\,2}$ following the model equations listed in Table 3b. The values are shown in Figs. 14–17 as a function of reactant partial pressure. Also, using the values of θ_{*H} from Fig. 15b, values of the elementary rate constant for acyl hydrogenation by metal chemisorbed hydrogen, $k_{acyl\,1}$, were estimated by

$$k_{acyl\,1} = k_{acyl\,1}/\theta_{*H} \quad [29]$$

and are shown in Fig. 16c.

k_{eth}, shown in Fig. 14a, reflects the activity of the ethane intermediates and ranges in value from just under 2 s^{-1} to just over 13 s^{-1}, averaging about 8 s^{-1}. Comparing these values with those of k_H in Fig. 15a, which reflect CO insertion activity, quantitatively demonstrates that the k_{eth} values are more than two orders of magnitude higher than the k_H values throughout the entire range of reactant partial pressures.

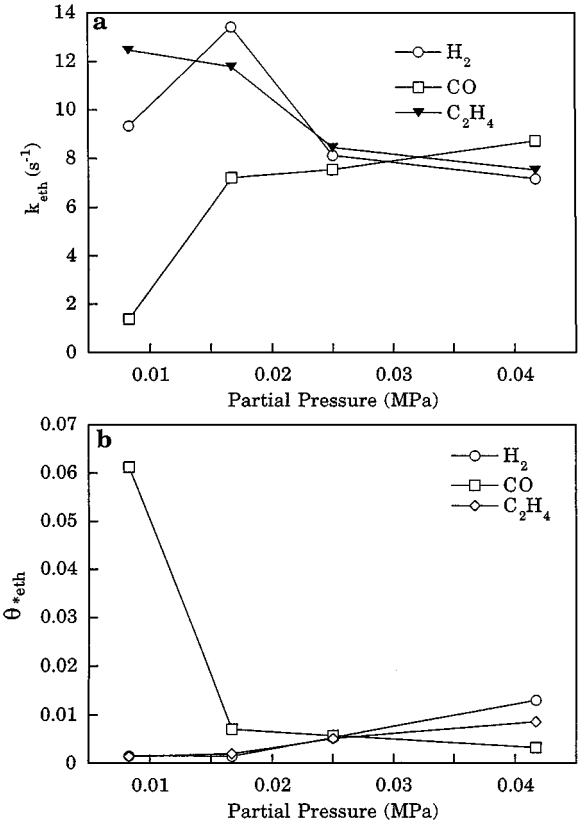

FIG. 14. (a) k_{eth} and (b) θ_{*eth} versus reactant partial pressure.

TABLE 3b

Parameters Determined by Model Equations

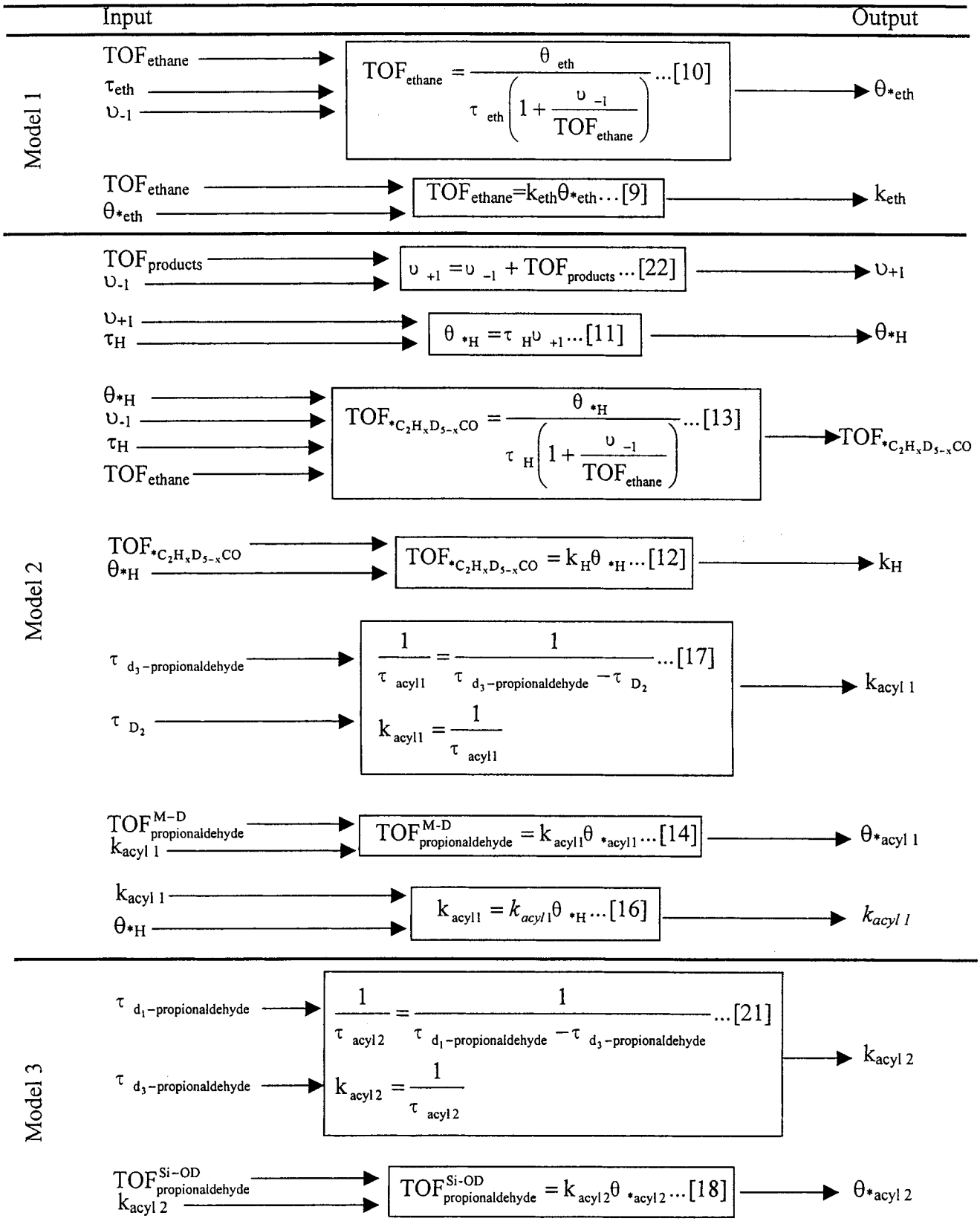

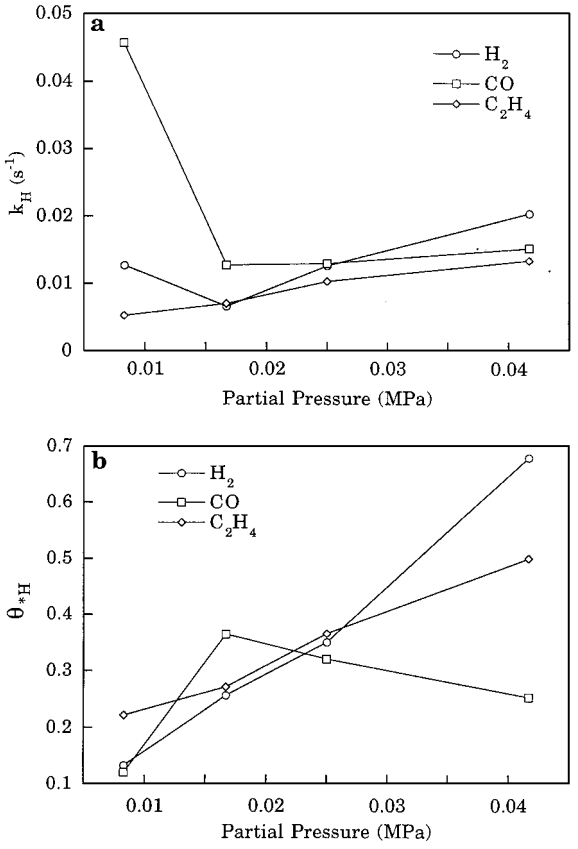

FIG. 15. (a) k_H and (b) θ_{*H} versus reactant partial pressure.

Propionaldehyde formation, as shown in Fig. 11, involves (i) k_H, the rate coefficient for conversion of pool 1 intermediates corresponding to the CO insertion step, (ii) $k_{acyl\,1}$, the rate coefficient for conversion of adsorbed acyl intermediate corresponding to hydrogenation via metal-chemisorbed hydrogen, and (iii) $k_{acyl\,2}$, the rate coefficient for conversion of adsorbed acyl intermediate corresponding to hydrogenation via spillover hydrogen. Comparing k_H in Fig. 15a with $k_{acyl\,1}$ in Fig. 16a yields information about the rate limiting step for propionaldehyde formation. $k_{acyl\,1}$ is, on average, about an order of magnitude higher than k_H, suggesting that CO insertion is the slow step. k_H remains the slow step through the entire range of reactant partial pressures. However, $k_{acyl\,1}$ is also an order of magnitude higher than $k_{acyl\,2}$ (shown in Fig. 17a), the rate coefficient for acyl hydrogenated via spillover hydrogen, indicating hydrogenation via metal-chemisorbed hydrogen is the favored path. Lack of a significant difference (i.e., more than three orders of magnitude) between k_H and $k_{acyl\,1}/k_{acyl\,2}$ suggests the absence of a clear rate-limiting step; acyl hydrogenation and CO insertion are both kinetically significant, which is consistent with a previous study that utilized the Langmuir–Hinshelwood–Hougen–Watson (LHHW) and pseudo-steady-state analysis (PSSA) approaches (17).

Our previous kinetic and ^{13}CO pulse transient studies have shown that the role of Mn is to shift the rate-limiting step from hydrogenation of acyl species and to blur the rate-limiting step in propionaldehyde formation (17, 18). Shifting of the rate-limiting step from hydrogenation by Mn species can be attributed to its promotion of CO insertion. MnO has been postulated to be an oxophilic promoter which interacts with the oxygen end of adsorbed CO on Rh giving a tilted CO, thus promoting its CO insertion (33). However, our transient IR studies show that tilted CO is a spectator (34). Due to lack of knowledge of the chemical state of Mn and its distribution on the catalyst surface, how

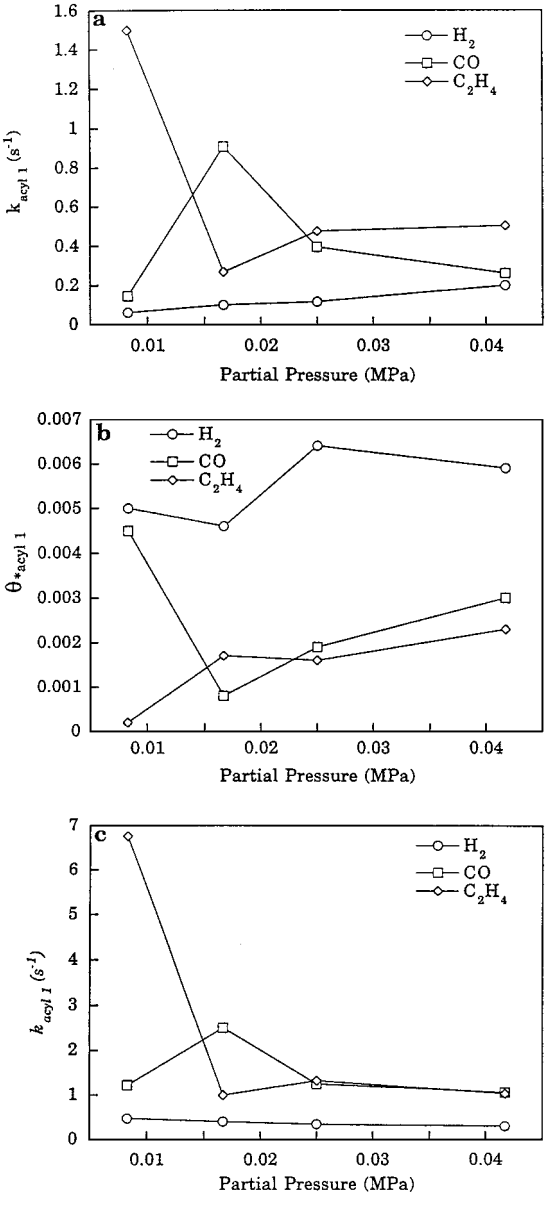

FIG. 16. (a) $k_{acyl\,1}$, (b) $\theta_{*acyl\,1}$, and (c) $k_{acyl\,1}$ versus reactant partial pressure.

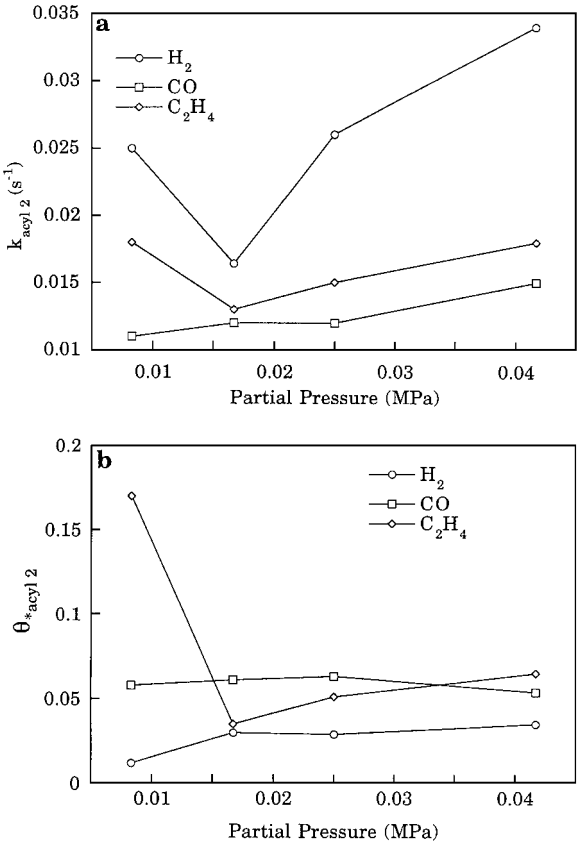

FIG. 17. (a) k_{acyl2} and (b) θ_{*acyl2} versus reactant partial pressure.

the Mn species interacts with the reaction intermediates and shifts the rate-limiting step remains in a speculation stage.

From reaction kinetics, the elementary rate constant has been shown only to be a function of temperature and independent of reactant partial pressure. However, Fig. 16c shows that the true rate constant k_{acyl1} varies with reactant partial pressure at constant temperature. This variation suggests (i) changes in the intrinsic activity and the rate-limiting step due to changes in adsorbate coverages and/or (ii) the θ_{*H} term in Eq. [16] is not first order. Current data are not available to distinguish the exact cause of variation.

The coverage of intermediates leading to ethane formation, θ_{*eth}, shown in Fig. 14b, is very small, with all values below 0.01 except two. These values lie within the same order of magnitude as θ_{*acyl1} shown in Fig. 16b, an order of magnitude below θ_{*acyl2} shown in Fig. 17b, and two orders of magnitude below θ_{*H} shown in Fig. 15b.

The reproducibility of the results shown in Figs. 13–17 is reflected by the runs where all reactant partial pressures are equal at 0.025 MPa. Three identical runs were performed at these conditions, so they act as a gauge for estimating the degree of experimental error and reproducibility of the data. Figures 13a, 14, and 15 exhibit very little difference in the values for the three 0.025 MPa runs, indicating excellent precision. However, the remaining figures do show a degree of spread for these particular runs. Figure 13b, which shows the hydrogen desorption rates, varies from 0.02 to 0.027. Figures 16a–16c, which show the rate parameters for the second pool of Model 2, show variation from 0.1 to 0.5, 0.0016 to 0.0064, and 0.2 to 1.3, respectively. Figures 17a and 17b, which show the model parameters for the second pool of Model 3, show variation from 0.012 to 0.026 and 0.035 to 0.065, respectively.

D_2 versus ^{13}CO Pulse Tracing

Pulse injection of deuterium allowed tracing of the deuterium pathway in ethane and propionaldehyde formation while the ^{13}CO pulse follows the ^{13}C pathway in propionadehyde formation. Figure 18 summarizes the key features of isotopic responses. As pointed out in the model development, elucidation of the mechanism requires the use of compartment modeling with proper postulations. One unique feature of the pulse transient technique is to determine the coverage of adsorbed intermediates which can be used for analysis of adsorbed intermediate isotherm equations in LHHW and PSSA kinetics. However, due to the inability to separate θ_{*H} and θ_{*eth} as well as complication from the θ_{*acyl1} and θ_{*acyl2}, we are not able to employ LHHW and PSSA approaches for analysis of our D_2 tracing results.

CONCLUSIONS

SSITKA coupled with *in situ* IR allows determination of rate coefficients, elementary rate constants, surface coverages, and residence times of surface intermediates. Compartment models for ethane and propionaldehyde formation were developed and their corresponding rate parameters were calculated versus reactant partial pressure from the reactant and product transient responses. Accurate determination of these parameters requires reasonable estimates for the steady-state rates of desorption and adsorption of hydrogen. A novel method utilizing the uniqueness of the HD transient from the D_2 pulse input was developed to estimate these rates. The rate estimates for hydrogen desorption were compared with those calculated from transition state theory and showed remarkable agreement.

Evaluation of rate coefficients indicates that hydrogenation of adsorbed ethyl is intrinsically faster than CO insertion into ethyl, leading to the high selectivity toward ethane over propionaldehyde as product. The propionaldehyde compartment models were able to account for two modes of acyl hydrogenation: (i) from $^*H$ on the metal surface and (ii) from spillover $^*H$, or Si–OH. Hydrogenation via metal-adsorbed hydrogen is favored over

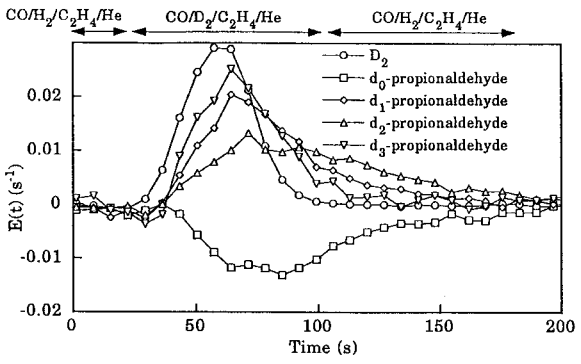

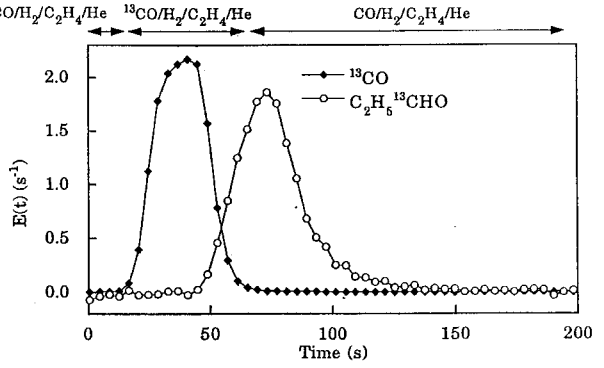

OBSERVATIONS

Isotope – containing products are $C_2H_xD_{6-x}$ and $C_2H_xD_{6-x}CO$; d_i – ethane responses led d_i – propionaldehyde responses; two - hump propionaldehyde response was the result of deuteration pathways; acyl hydrogenation / deuteration can occur by metal - adsorbed hydrogen / deuterium and by spillover hydrogen / deuterium; $C_2H_xD_{6-x}CO$ response was modeled by two - pool model; $\theta_{pool\ i}$ was determined from equations in Table 2

OBSERVATIONS

Isotope - containing product is $C_2H_5{}^{13}CHO$; $C_2H_5{}^{13}CHO$ response was modeled by a one - pool model;

$\theta_{intermediates} = \tau_{C_2H_5{}^{13}CHO} \bullet TOF_{C_2H_5CHO}$

MODEL

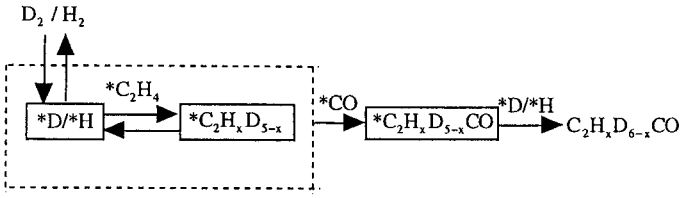

MODEL

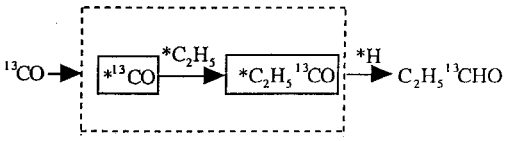

FIG. 18. D_2 versus ^{13}CO pulse transients.

hydrogenation via spillover hydrogen. Comparison of the rate coefficients for CO insertion and acyl hydrogenation indicate that both steps are kinetically signficant, which is consistent with previous studies that utilized the Langmuir–Hinshelwood–Hougen–Watson and pseudo-steady-state analysis approaches.

Kinetic studies of reactions on catalyst surfaces may be divided into three levels: (i) determination of the macroscopic rate law from steady-state data, (ii) LWWH and PSSA kinetics, and (iii) determination of the elementary rate law. Accurate evaluation of kinetic parameters for each level is increasingly more difficult and fundamental. This study has provided reasonable estimates for intermediate surface coverages, rate coefficients, and elementary rate constants. Variation of the elementary rate constant $k_{acyl\,1}$ was observed with changing reactant partial pressure, suggesting (i) changes in intrinsic activity occur due to changes in adsorbate coverages or (ii) θ_{*H} in Eq. [16] is not actually first order. Accurate determination of elementary rate parameters requires further improvement in time resolution of SSITKA as well as refinement of the model for the reaction.

ACKNOWLEDGMENTS

The authors gratefully acknowledge the partial support of this research by the National Science Foundation under Grant CTS-9421119996 and the Ohio Board of Regents Research Challenge Grant.

REFERENCES

1. Rabo, J., *in* "Proceedings, 10th International Congress on Catalysis, Budapest, 1992" (L. Guczi, F. Solymosi, and P. Tetenyi, Eds.). Akadémiai Kiadó, Budapest, and Elsevier Science, Amsterdam, 1993.
2. Chuang, S. S. C., Brundage, M. A., Balakos, M. W., and Srinivas, G., *Appl. Spectrosc.* **49**, 1151 (1995).
3. Balakos, M. W., Chuang, S. S. C., Srinivas, G., and Brundage, M. A., *J. Catal.* **157**, 51 (1995).
4. Hoost, T. E., and Goodwin, J. G., Jr., *J. Catal.* **137**, 22 (1992).
5. Siddall, J. H., Miller, M. L., and Delgass, W. N., *Chem. Eng. Comm.* **83**, 261 (1989).
6. Stockwell, D. M., Bianchi, D., and Bennett, C. O., *J. Catal.* **113**, 13 (1988).
7. Mims, C. A., and McCandlish, L. E., *J. Phys. Chem.* **91**, 929 (1987).
8. de Pontes, M., Yokomizo, G. H., and Bell, A. T., *J. Catal.* **104**, 147 (1987).
9. Biloen, P., Helle, J. N., van den Berg, F. G. A., and Sachtler, W. M. H., *J. Catal.* **81**, 450 (1983).

10. Kobori, Y., Yamasaki, H., Naito, S., Onishi, T., and Tamaru, K., *J. Chem. Soc., Faraday Trans. 1* **78**, 1473 (1982).
11. Happel, J., Suzuki, I., Kokayeff, P., and Fthenakis, V., *J. Catal.* **65**, 59 (1980).
12. Ponec, V., and Bond, G. C., *in* "Catalysis by Metals and Alloys" (B. Delmon and J. T. Yates, Eds.), Vol. 95, p. 449. Elsevier, New York, 1995.
13. Goddard, S. A., Cortright, R. D., and Dumesic, J. A., *J. Catal.* **137**, 186 (1992).
14. Watson, P. R., and Somorjai, G. A., *J. Catal.* **74**, 282 (1982).
15. Balakos, M. W., and Chuang, S. S. C., *J. Catal.* **151**, 253 (1995).
16. Balakos, M. W., and Chuang, S. S. C., *J. Catal.* **151**, 266 (1995).
17. Brundage, M. A., Balakos, M. W., and Chuang, S. S. C., *J. Catal.* **173**, 122 (1998).
18. Brundage, M. A., Chuang, S. S. C., and Hedrick, S. A., *Catalysis Today* **44**, 151 (1998).
19. Brundage, M. A., and Chuang, S. S. C., *J. Catal.* **164**, 94 (1996).
20. Brundage, M. A., Ph.D. Dissertation, The University of Akron, 1997.
21. Levenspiel, O., "Chemical Reaction Engineering." Wiley, New York, 1972.
22. Kemball, C., *J. Chem. Soc.* **735**, (1956).
23. Bond, G. C., Philipson, J. J., Wells, P. B., and Winterbottom, J. M., *Trans. Faraday Soc.* **62**, 443 (1966).
24. Shannon, S. L., and Goodwin, J. G., Jr., *Chem. Rev.* **95**, 677 (1995).
25. Cremer, P., Su, X., Shen, Y., and Samorjai, G., *J. Am. Chem. Soc.* **118**, 2492 (1996).
26. Mazanec, T., *J. Catal.* **98**, 115 (1986).
27. Hedrick, S. A., M.S. thesis, The University of Akron, 1998.
28. Dumesic, J. A., Rudd, D. F., Aparicio, L. M., Rekoske, J. E., and Treviño, A. A., "The Microkinetics of Heterogeneous Catalysis." Amer. Chem. Soc., Washington, DC, 1993.
29. Stuve, E. M., and Madix, R. J., *J. Phys. Chem.* **89**, 105 (1985).
30. Lombardo, S. J., and Bell, A. T., *Surf. Sci. Rep.* **13**, 1 (1991).
31. Stuchly, V., and Klusácek, K., *J. Catal.* **139**, 62 (1993).
32. Olivé, G. H., and Olivé, S., "The Chemistry of the Catalyzed Hydrogenation of Carbon Monoxide." Springer-Verlag, New York, 1984.
33. Sachtler, W. M. H., *in* "Proceedings, 8th International Congress on Catalysis, Berlin, 1984." Dechema, Frankfurt-am-Main, 1984.
34. Chuang, S. S. C., Brundage, M. A., and Balakos, M. W., *Appl. Catal. A: General* **151**, 333 (1997).